2004 ASME/STLE International Joint Tribology Conference
Long Beach, California USA, October 24-27, 2004

TRIB2004-64199

EXPERIMENTAL AND THEORETICAL STUDY OF INSTANTANEOUS PISTON ASSEMBLY FRICTION IN A GASOLINE ENGINE

Riaz A Mufti[a], Martin Priest[b] and Richard J Chittenden
Institute of Tribology
School of Mechanical Engineering
The University of Leeds
Leeds LS2 9JT, UK

[a]corresponding address: Castrol Technology Centre, Pangbourne. Reading RG8 7QR, UK. Tel: +44 (0)118 9765434, email: muftr1@bp.com

[b]corresponding author tel: +44 (0)113 3432178 fax: +44 (0)113 2424611, email: M.Priest@leeds.ac.uk

ABSTRACT

A piston assembly friction model has been developed to predict the individual performance of compression rings, the oil control ring and the piston skirt. Validation of this model has been undertaken by comparing the predicted results with the experimental measurements of piston assembly friction in a gasoline engine under fired conditions using the IMEP (indicated mean effective pressure) method. The experimental results for an SAE 0W20 without friction modifier were compared with the predictions. The predicted results correlate very well with the measurements, especially at higher lubricant inlet temperatures. Piston skirt friction was predicted using both a simple concentric piston / cylinder model and a more realistic but computationally intensive method incorporating piston secondary motion. The results clearly indicate that the latter more realistic method is required to achieve satisfactory correlation with the measured data.

1 INTRODUCTION

A significant part of internal combustion engine mechanical power loss is due to piston assembly/cylinder bore friction Dowson [1] and this has a great influence on fuel economy. The losses arise from the interaction between the cylinder liner, compression rings, oil control ring and piston skirt. Piston ring lubrication models have been under development for many years. In an early investigation, Furuhama [2] carried out the lubrication analysis for a single piston ring whereas Lloyd [3] demonstrated that an optimum ring profile existed that maximised the oil film thickness for a given engine conditions. Wakuri et al [4] considered the effects of cavitation and squeeze film on ring analysis. These were also considered by Dowson et al [5] for the complete compression ring pack along with the influence of lubricant starvation. Ruddy [6] extended this work and included mixed lubrication analysis.

Compared to piston ring lubrication analysis, piston skirt lubrication has received little attention. The piston throughout the combustion cycle exhibits significant secondary motions. Lateral movement across the cylinder and rotation about the gudgeon pin causes the piston to tilt in the bore, as described by Chittenden and Priest [7].

Based on such research work, a piston assembly friction model was developed by Yang [8] and later modified by Dickenson [9], at the authors Institution, assessing the individual performance of the piston, compression rings and the oil control ring. The piston skirt analysis was based on a very simple model, calculating the shear losses by assuming that the piston and the cylinder are concentric. A more realistic and complex piston skirt model has been developed by Chittenden and Priest [7], based on the work of Li et al [10]. This paper compares the predictions of these models with measured piston assembly friction on a fired gasoline engine.

The Piston assembly friction loss was measured under fired conditions on a single cylinder Ricardo Hydra gasoline engine

using the IMEP method, Mufti and Priest [11]. This method requires almost no major engine modification and thus gives a representative picture of piston/liner friction in a modern gasoline engine.

2 PISTON COMPRESSION RING FRICTION MODEL

To predict the performance of the piston assembly it is necessary to analyse each component separately. The compression rings act as a gas seal to the combustion chamber and there is a substantial variation of gas pressure throughout the ring pack during the engine cycle.

The lubrication analysis of a compression ring requires detailed understanding of all the forces acting on it. One of the main forces acting on the top compression ring is the combustion pressure force which can be determined relatively easily using a pressure transducer, whereas the measurement of inter-ring gas pressure is not an easy task. However, inter-ring gas pressure can be predicted using the so-called orifice and volume theory described below.

As noted above, the main purpose of the compression rings is to prevent leakage of gases from the combustion chamber. It is of course, acknowledged that a single ring cannot form a perfect seal and in most cases a ring pack is used to share the gas pressure gradient from the combustion chamber to crankcase. In spite of this, some gas leakage is still be expected to occur through the rings, known as blow by. If the ring is performing properly then the pressure of the oil film between the ring face and the liner will prevent this blow-by passing via this route. The piston ring can seal against the upper groove flank as well as the lower depending on the gas pressure acting on the ring top and bottom flank but practical and experimental experience suggests that in most cases the gas pressure loading on the top flank of the ring is greater than that on the lower flank thus pushing the ring against the groove lower surface during most of the working period but still there may be some gas leakage between the ring and its groove as this ideal condition does not always exist. Axial movement of the ring (ring flutter) due to unbalanced forces may cause excessive gas leakage. Despite the possibility of blow by due to ring flutter and ring lift and gas escaping past the face of the piston ring, it is acknowledged that the ring gaps are the primary route for gas leakage and thus are of most importance in determining the inter-ring gas pressures.

Eweis [12] was the first to propose the so-called orifice and volume model addressing engine blow by. Later the model was developed by Ting and Mayer [13] and applied extensively by Ruddy et al [14] and Kuo et al [15], and is now the popular way of predicting inter-ring gas pressures. The model assumes that the ring gaps are the only gas leakage paths and that the gas flow is an adiabatic flow. The ring pack comprises a series of square-edged orifices and adjacent volumes. This model is used as the basis for the present analysis.

To predict the inter-ring gas pressure using the orifice and volume method, two equations are required, equation for the flow rate through the orifice and an expression describing the rate of change of pressure within a volume.

In deriving the equation for the mass flow rate through the orifice it is assumed that the rate of heat transfer is sufficiently small for the flow to be assumed to be adiabatic. It is also assumed that the gas flow is isentropic and obeys the ideal gas law. Then the mass flow rate according to Yang [8] can be derived in non-dimensional form as

$$\frac{d\bar{m}_{n-1}}{dq} = K_i \left(\frac{A_n}{A_1}\right)\left[\frac{\bar{P}_{n-1}}{\sqrt{\bar{T}}_{n-1}}\right]\left(\frac{\bar{P}_n}{\bar{P}_{n-1}}\right)^{\frac{1}{g}}\left[1-\left(\frac{\bar{P}_n}{\bar{P}_{n-1}}\right)^{\frac{g-1}{g}}\right]^{\frac{1}{2}} \quad \text{.....(1)}$$

where, $K_i = \dfrac{K_c A_1}{V_1 w}\left[\dfrac{2gRT_o}{g-1}\right]^{\frac{1}{2}}$

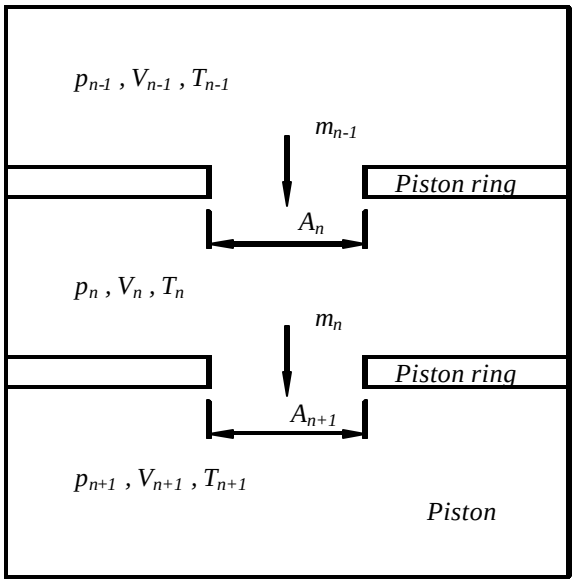

Figure 1. Ring pack gas flow, orifice and volume model for inter-ring gas pressure prediction.

According to figure 1, at any instant the pressure within a volume is given by the ideal gas

$$p_n = \frac{RT_n}{V_n}\left(m_i + m_{in} - m_{out}\right) \qquad (2)$$

where at any crank angle,
m_i, mass of gas in the inter-ring volume.
m_{in}, mass of gas entering the inter-ring volume region.
m_{out}, mass of gas leaving the inter-ring volume region.

Differenitating equation 2 and writing in non-dimensional form

$$\frac{d\bar{P}_n}{dq} = \bar{T}_n\left(\frac{V_1}{V_n}\right)\left(\frac{d\bar{m}_{n-1}}{dq} - \frac{d\bar{m}_n}{dq}\right) \qquad (3)$$

From equation 1 and 3, the inter-ring gas pressure can be predicted

$$\left(p_n\right)_{q+dq} = \left(p_n\right)_q + \frac{dq}{2}\left[\left(\frac{dp_n}{dq}\right)_q + \left(\frac{dp_n}{dq}\right)_{q+dq}\right] \quad \text{.....(4)}$$

At the critical pressure ratio, that is when the gas flow velocity across the orifice reaches the local speed of sound, equation 1 reduces to

$$\frac{d\bar{m}_{n-1}}{dq} = 0.227K_i\left(\frac{A_n}{A}\right)\left(\frac{p_{n-1}}{\sqrt{\bar{T}_{n-1}}}\right) \quad (5)$$

$\gamma = 1.3$ and the discharge coefficient K_c = 0.65 for a square edged orifice.

Based on equations 1 to 5 the inter-ring gas pressure between the compression rings can be predicted at each crank angle.

The compression rings are manufactured with a small spring force to force the ring against the liner, but this action is substantially enhanced by the gas pressure acting on the inner diameter of the ring. It is assumed that a thin oil film separates the compression rings from the liner and thus Reynolds equation can be used to determine the film thickness throughout the engine cycle. For the piston ring lubrication analysis and to solve the Reynolds equation it is necessary to determine the following parameters,

- Shape of the piston ring face in the direction of sliding.
- Piston ring sliding speed.
- Piston ring loading.
- Lubricant viscosity.

The model assumes that the surfaces of the liner and the rings are smooth and have good circumferential conformity. Hence no oil flows in circumferential direction due to lack of a pressure gradient or surface velocities, thus reducing the problem to two-dimensional case. Piston ring face adjacent to the liner are normally manufactured with a curved profile to assist in the lubrication. The ring twists during each cycle and wear also causes a curved profile to form on the face.

The bearing hydrodynamic lubrication is greatly influenced by the change in film thickness along the bearing length than by the form of the change and because of the ring face curved profile, the piston ring lubrication analysis can be achieved by representing the ring face by a curved profile of parabolic form as the effective radius of curvature of the ring face is much larger than the width of the ring. Thus according to figure 2, the shape of the ring face can be expressed as,

$$h(x) = h_{\min} + \frac{\left(x - x_{\min}\right)^2}{2R_r} \quad (6)$$

To calculate the lubricant film thickness at the liner/ring interface it is important to determine the entraining and sliding velocities. During an engine cycle, ring lift may occur in the piston groove due to the force balance. If this lift is reasonably neglected, the axial cyclic velocity of the ring can be assumed to be identical to that of the piston. Thus the axial velocity of the piston and hence the piston rings is given by,

$$U_r = R_a w\left[\sin q + \frac{\sin 2q}{2\left(\left(\frac{L}{R_a}\right)^2 - \sin^2 q\right)^{\frac{1}{2}}}\right] \quad (7)$$

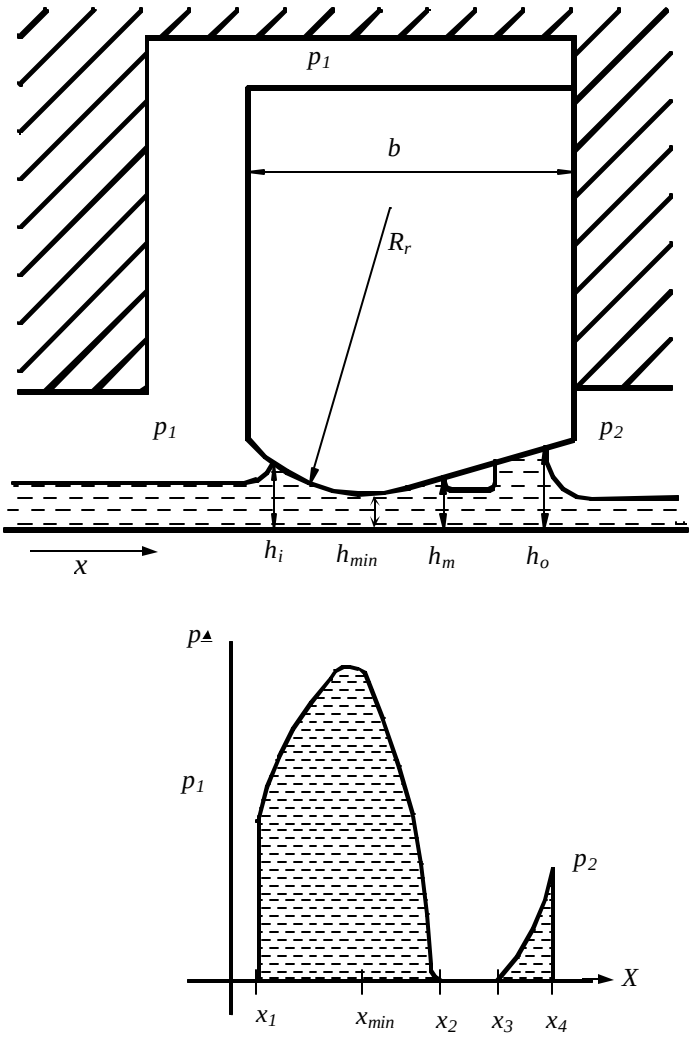

Figure 2. Hydrodynamic film shape and pressure distribution at the compression ring and cylinder liner interface.

To solve Reynolds equation, it is considered that the liner transports the lubricant, that is the piston ring remain stationary and the cylinder liner moves past the ring at the speed of the piston. The equivalent liner velocity U_l is then equal in magnitude but opposite in direction to the sliding velocity of the piston rings. According to figure 2, it is assumed that pressure p_1 is greater than pressure p_2 and thus the pressure p_1 is applied at the back of the ring. If p_2 is greater than p_1, the ring is assumed to move to the other flank of the ring groove resulting in pressure p_2 being applied at the back of the piston ring.

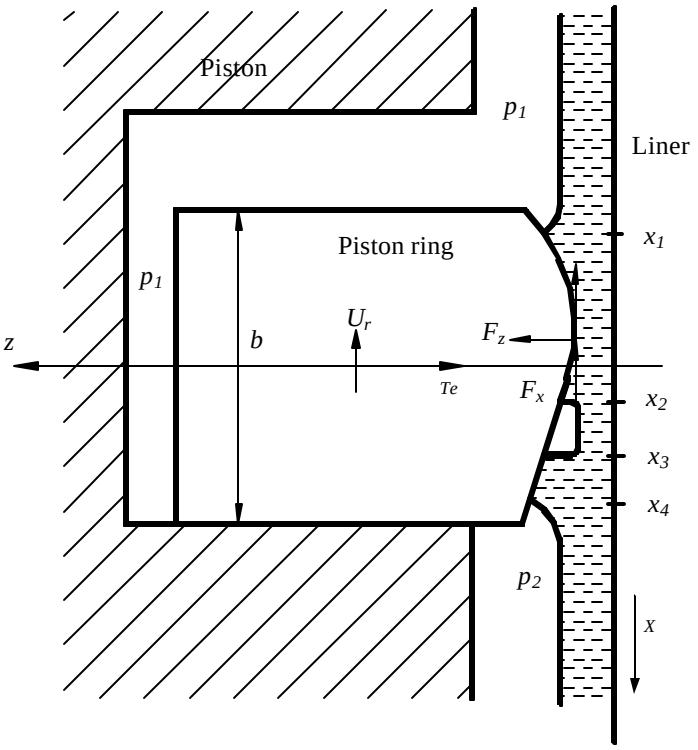

Figure 3. Forces acting on a single piston ring.

The forces acting on the piston ring according to figure 3 are,

- Gas force above and below the ring.
- Viscous traction and lubricant pressure force within the film.
- Piston ring elastic tension.
- Reaction from the contacting flank between the ring and the piston ring groove.

It is assumed in the present study that the net radial force is supported by the hydrodynamic action in the oil film produced by the entraining velocity and squeeze action. If the lubricant supply is insufficient to flood the ring, part of the ring face will be exposed to the gas pressure above and below the ring, p_1 and p_2 figure 3. If the radial friction force between the ring and the groove and the ring radial inertia are neglected, the hydrodynamic force is then balanced as,

$$F_z = p_1\left(b - x_1\right) - p_2\left(b - x_4\right) + T_e b \qquad (8)$$

It is assumed that the viscosity of the lubricant film varies according to the axial temperature variation of the cylinder liner. Knowing the cylinder liner measured near surface temperature at several points, the intermediate temperature values along the liner at any point in a stroke can be interpolated. If the appropriate viscosity-temperature characteristics of the lubricant are provided, the viscosity of the lubricant film between the ring and cylinder liner can be calculated at any crank angle. In this research nine thermocouples were fitted on the liner to monitor the liner near surface temperature at TDC, BDC and mid stroke, Mufti and Priest [11].

The parabolic shape of the ring and the straight liner produces a convergent/divergent clearance, assuming that the liner transports the lubricant. The divergent region will theoretically produce a sub-ambient pressure profile. In reality, the lubricant cannot withstand pressures below saturation level without releasing dissolved gases or pressures below vapour pressure without boiling and this will result in film rupture called cavitation. Gumbel [16] recognised the inability of the fluid to sustain large and continuous negative pressures and believed to be effectively producing a cavitation region, assuming all negative pressures are set to zero. Thus Reynolds cavitation boundary condition can be applied in this region. The experimental evidence of cavitation has been reported by Brown and Hamilton [17].

Referring to figure 2 the pressure within the oil film at the entraining inlet, at location x_1 must equal the gas pressure p_1. The oil pressure due to the wedge effect rises fom p_1 at location x_1 to a maximum and then falls to atmospheric or saturation pressure due to cavitation at the point of film rupture x_2, where the film thickness is defined by h_m. If pressure p_2 at the trailing edge of the ring is significant, the oil film must reform at some location x_3 so that a positive pressure can be reached to the boundary pressure p_2 at the trailing outlet at some location x_4 where the film thickness is defined as h_o. Thus three pressure regions can be defined along the ring face, a positive pressure region where the pressure varies from p_1 at x_1, to atmospheric at x_2, a cavitation region from x_2 through to x_3 where the film ruptures and the pressure is constant, normally taken as atmospheric, and finally the third region from x_3 to x_4 where the oil film may redevelop and the pressure rises from atmospheric pressure to pressure p_2. For the piston ring lubrication analysis it is vital to determine these pressures and locations using Reynolds equation.

Reynolds equation is the governing equation for the pressure distribution in a fluid film bearing. The three dimensional incompressible Reynolds equation is expressed as,

$$\frac{\partial}{\partial x}\left(h^3\frac{\partial p}{\partial x}\right)+\frac{\partial}{\partial y}\left(h^3\frac{\partial p}{\partial y}\right)=6h\left\{\frac{\partial}{\partial x}\left(U_1+U_2\right)h+\frac{\partial}{\partial x}\left(V_1+V_2\right)h+2\left(w_h-w_o\right)\right\} \qquad \text{.....(9)}$$

For the present piston ring/liner interface the above equation can be simplified assuming that the velocity of piston ring and the change of oil film thickness along the circumferential direction is zero. Thus $U_2 = 0$ and liner velocity $U_1 = U_l$, as explained previously. Also substituting $(w_h - w_o)$ with $\dfrac{\partial h}{\partial t}$, as the surfaces are impermeable so no fluid seeps in or out. The reduced form is given by,

$$\frac{\partial}{\partial x}\left(h^3\frac{\partial p}{\partial x}\right)=6h\left\{U_l\frac{\partial h}{\partial x}+2w\frac{\partial h}{\partial q}\right\} \qquad (10)$$

In the above equation the left-hand side represents the variation of pressure in the *'x'* direction that is the direction of liner motion.

The first term in the right-hand side describes the normal wedge action whereas the second term expresses the squeeze film effect. The integration of the above equation gives an expression for the axial pressure gradient for the inlet region,

$$\frac{dp_a}{dx} = \frac{1}{h^3}\{6hU_l + 12hw + C_1\} \qquad (11)$$

The hydrodynamic pressure within the lubricating film in the inlet region can be calculated by integrating equation 11,

$$p_a = 6hU_l I_1 + 12hw\frac{dh}{dq}I_2 + C_1 I_3 + C_2 \qquad (12)$$

where

$$I_1 = \int \frac{1}{h^2}dx,\ I_2 = \int \frac{x}{h^3}dx,\ I_3 = \int \frac{1}{h^3}dx \text{ and } C_1, C_2$$

are integration constants.

For the ring of parabolic profile, the integrals, I_1, I_2, and I_3 have analytical solutions. A solution of equation 12 requires that the integration constants C_1 and C_2 and the cavitation and reformation locations x_2 and x_3 should be determined.

Constants C_1 and C_2 and location x_2 can be determined by applying the following boundary conditions to equation 11 and 12.

$p_a = p_1$ at $x = x_1$

$p_a = \frac{dp_a}{dx} = 0$ at $x = x_2$

The reformation boundary x_3 can be determined by considering the continuity of flow and the boundary pressure conditions at the trailing edge of the ring. According to Reynolds equation, the expression for the volume rate of flow per unit circumferential length for the present case is given by

$$Q = -\frac{h^3}{12h}\frac{dp}{dx} + \frac{U_l h}{2} \qquad (13)$$

Also the flow rate per unit length at the cavitation boundary x_2 can be expressed as,

$$\frac{U_l h_m}{2} \qquad (14)$$

since $\frac{dp}{dx} = 0$.

This flow rate at the cavitation boundary must be equal to that past the outlet region of the ring. Thus equating equation 13 to 14,

$$\frac{dp_b}{dx} = 6hU_l\left(\frac{h - h_m}{h^3}\right) \qquad (15)$$

where 'p_b' is the hydrodynamic pressure in the region between x_3 and x_4. Integrating the above equation and applying the following boundary conditions, the integration constant and the reformation location x_3 can be calculated.

$p_b = p_2$ at $x = x_4$

$p_b = 0$ at $x = x_3$

Knowing the entire integration constants and the cavitation and reformation boundary locations, the oil pressure p_a in the region x_1 and x_2 in front of the cavitation region and the oil pressure p_b in the area x_3 and x_4 behind the cavitation region can be calculated. Thus the hydrodynamic radial force per unit length F_z, can be determined by direct integration as

$$F_z = \int_{x_1}^{x_2} p_a dx + \int_{x_3}^{x_4} p_b dx \qquad (16)$$

This force is equal to the load applied radially on the ring as expressed by equation 8. Combining equation 8 and equation 16, the change of film thickness with respect to crank angle $\frac{dh}{dq}$ can be calculated. Both the quantities $\frac{dh}{dq}$ and h_{min} are not known initially. $\frac{dh}{dq}$ can be calculated if an initial estimate is made of h_{min} at some crank angle where the film thickness is expected to change only slowly wiyh crank angle. Once $\frac{dh}{dq}$ is known, values of h_{min} can be calculated for a complete engine cycle using the well-known Trapezoidal rule,

$$h_{q+dq} \approx h_q + \frac{dq}{2}\left[\left(\frac{dh}{dq}\right)_q + \left(\frac{dh}{dq}\right)_{q+dq}\right] \qquad (17)$$

where h_q is the minimum film thickness at crank angle q and dq is the crank angle increment.

If the calculated film thickness at each crank angle is found to be greater than the composite roughness of the ring and cylinder liner, it is assumed the ring is operating in the hydrodynamic regime and the friction is due to the shearing of the fluid. The friction force per unit circumferential length is determined as,

$$F_r = \int_{x_1}^{x_4}\left(h\frac{du}{dz}\right)dx \qquad (18)$$

where the velocity gradient according to Cameron [18], for static piston ring and movable liner in the presence of lubricant pressure difference in x-axis direction is given by

$$\frac{du}{dz} = \frac{h}{2h}\frac{dp}{dx} + \frac{U_l}{h}$$

Thus equation 18 can be expressed, according to the boundary locations as,

$$F_r = \int_{x_1}^{x_2}\left(-\frac{h}{2}\frac{dp_a}{dx}+h\frac{U_l}{h}\right)dx+\int_{x_3}^{x_4}\left(-\frac{h}{2}\frac{dp_b}{dx}+h\frac{U_l}{h}\right)dx \quad \text{……(19)}$$

The average frictional power loss for a compression ring over one complete engine cycle is then given by,

$$H_r = \frac{1}{2p}\int_0^{2p} F_r p\, DU_l dq \quad (20)$$

where D is the engine cylinder bore diameter.

It is known that the predicted film thickness generally falls below the composite surface roughness for the ring and liner near both the piston dead center positions. Under such conditions boundary lubrication is assumed to occur and a constant coefficient of friction of 0.12 is applied for the SAE 0W20 without friction modifier.

In the present study it is assumed that the only way for oil to pass the piston rings is between the ring face and the cylinder liner. The lubricant flow rate can be calculated at the point where only Couette flow takes place, that is $\frac{dp}{dx}=0$. Thus the volume flow rate of lubricant *'Q'*, per unit width at any crank angle is given by,

$$Q = \frac{1}{2}U_l h_m \quad (21)$$

Integration of this quantity with respect to crank angle over the complete engine cycle gives the net volume rate of flow of lubricant. The sign of this net flow indicates whether the oil flows towards the combustion chamber or towards the crankcase.

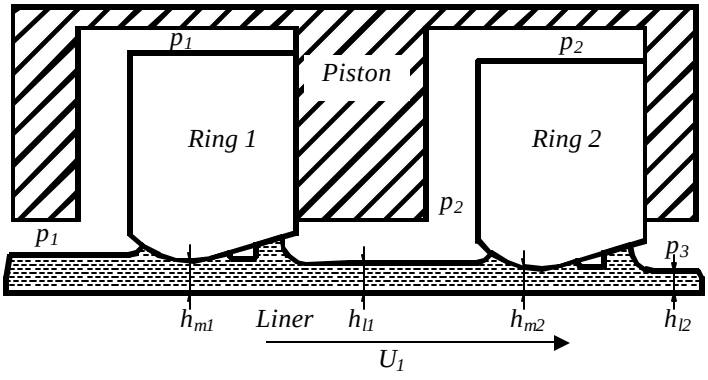

Figure 4. Lubricant flow in a piston ring pack

In most cases the sealing of the combustion chamber is made more effective by having more than one compression ring and the lubrication of the rings and the cylinder liner largely depends on the interaction of the ring pack. If plentiful lubricant is available at the inlet edge of the ring, the ring is said to have fully flooded lubrication, but if the inlet region is not flooded than the ring is said to undergo starved lubrication. Starvation for two adjacent compression rings working in a pack is shown in figure 4. The oil film thickness for the first ring is calculated by the method described earlier.

To calculate the film thickness for the second ring it is important to determine the oil film thickness left by the first ring and its effect on the position of the inlet boundary of the second ring. The information is then used to evaluate the film thickness for the second ring. According to the principle of continuity, the volume rate of flow past the second ring cannot exceed that past the first ring in the absence of any oil supply between the rings.

The magnitude of volume flow rate past the first ring is given by equation 21. The same quantity of oil must flow through the inter-ring region with velocity U_l. If the thickness of the film in the inter-ring region of the liner is h_l figure 4, and with no fresh supply of oil available, then

$$\frac{U_l h_m}{2} = U_l h_l \quad (22)$$

For the lubrication analysis of the ring pack it is initially assumed that *ring 1* is fully flooded and the lubrication theory for a single ring is used to determine film thickness h_m and minimum film thickness h_{min}. Using equation 22, the film thickness in the inter-ring region is calculated which is then available for *ring 2*. The film thickness may not be sufficient to flood *ring 2* and this may disturb the location of the inlet boundary. Thus an iterative procedure is used to determine the inlet boundary. Initially the minimum film thickness at each crank angle for all rings is calculated assuming all rings are fully flooded. The thickness of the oil film available for *ring 2* is then assumed to be h_{min} of *ring 1.* This film information is then used to calculate the initial location of the inlet boundary of *ring 2* and using the lubrication theory for a single ring, h_{min} and flow rate pass *ring 2* is calculated. The continuity equation 22 is then used to check the flow rate. If the continuity equation is not satisfied the film thickness at the inlet boundary to ring 2 is progressively reduced and the procedure is repeated until the continuity equation of flow is satisfied.

As mentioned above for the ring pack analysis it is assumed that the top ring is fully flooded but this may not be the case. Modern engines are splash lubricated from the sump and thus the fully flooded assumption can be true for the bottom ring during downward stroke. The lubrication of top ring purely relies on the net upward travel of oil through the ring pack and therefore it is assumed that the lubricant available for the top on the upstrokeis the lubricant left by it on the liner during downstroke. Thus for the top ring the continuity flow equation on the upstrokecan be expressed as

$$Q_{upstroke} \leq Q_{downstroke}$$

Where 'Q' is the volume flow rate per unit circumferential length.

3 OIL CONTROL RING FRICTION MODEL

Along with the compression rings one more ring is usually fitted in the groove near the upper end of the piston skirt, the oil control ring. The function of this ring is to restrict the amount of oil available to the compression rings and to distribute oil circumferentially around the liner. The working face of the oil control ring is normally narrower than the compression rings

and the tangential load is greater. It is therefore assumed that the control rings work in the mixed to boundary lubrication regime. Thus for the present study boundary lubrication is assumed and the friction is equal to the product of the normal load and a coefficient of friction (0.12 for SAE 0W20 without friction modifier). The normal load for the oil control ring is assumed to be only due to the elastic tension of the ring.

4 PISTON SKIRT FRICTION MODEL

The clearance between the piston and the liner varies along the piston axis due to the barrel shape of the piston required to accommodate the severe temperature gradient from the combustion chamber to the crankcase and to prevent edge loading on tilted pistons. Due to the relatively light loading and large contact area, the piston skirt normally operates in the hydrodynamic lubrication regime, Thring [19]. A very simple piston skirt power-loss analysis was used by Yang [8], assuming that the piston remains concentric with the cylinder liner axis throughout the cycle and that resistance to motion is caused by the shearing of the lubricant filling the clearance between the piston and the liner. An average piston/liner clearance value was applied through out the engine cycle. Thus the total piston skirt power-loss due to the viscous shear of lubricant at any instant can be calculated as

$$F_{skirt} = \int_0^{L_S} \frac{hU_l}{c} dx \qquad (23)$$

Where '*c*' is the radial clearance and 'L_S' is the piston skirt length. The local liner temperature reading determines the axial variation of lubricant viscosity.

A much more realistic approach has been used for piston skirt friction calculation lifting the assumption that the piston remains concentric in the liner resulting in complex analysis of piston motion. The primary movement of a piston is up and down the cylinder but there my also be significant secondary movement as it rotates around the gudgeon pin causing the piston to tilt within the cylinder or translates across the cylinder resulting in a larger clearance on one side of the bore than the other. This secondary motion can result in surface contact between the skirt and liner causing an increase in friction force, Nakayama et al [20]. Models have been developed by Chittenden and Priest [7] and Dursunkaya et al. [22] to study this secondary motion and to investigate the influential factors of load, speed, piston clearance and gudgeon pin offset. Details of the former are outlined here.

The piston skirt analysis links the piston dynamics with the hydrodynamic action of the lubricant surrounding the skirt. The influence of the latter adds additional components to the forces and moments governing the calculation of the piston dynamics. As shown in figure 5, they may be divided into four main groups:

(a) the forces acting in the axial direction and arising from the reciprocating action of the piston and the gas pressure on the piston crown [F_{pin}, F_{cg}, F_G and also a component of M_I]

(b) hydrodynamic forces and moment acting against the transverse motion of the piston [G_H, M_H and G_{pin}]

(c) inertia forces acting in the transverse direction due to the transverse accelerations of the piston [G_{cg} and a component of M_I]

(d) forces acting along the connecting rod, which may be attributed to the reciprocating mass of the piston assembly [F_{rod}]

Having established the forces and moments acting upon the piston the equations of motion may be written for both the axial (X) and transverse (Y) directions as follows:-.

$$F_G + F_{cg} + F_{pin} + F_{rod}\cos\phi = 0 \qquad (24)$$

$$G_H + G_{pin} + G_{cg} - F_{rod}\sin\phi = 0 \qquad (25)$$

Taking moments about the gudgeon pin:-

$$M_I + M_H - F_{cg}y_{cg} + F_G y_{pin} + G_{cg}\left(x_{pin} - x_{cg}\right) = 0 \qquad \ldots\ldots\ldots\ldots\ldots\ldots (26)$$

Note, the reciprocating inertia forces for a constant crankshaft speed (ω) are given by:-

$$F_{cg} = -m_{pis}\ddot{x} \qquad (27)$$

$$F_{pin} = -m_{pin}\ddot{x} \qquad (28)$$

where $\ddot{x}$ is given by the standard expression for piston axial acceleration derived from the engine geometry.

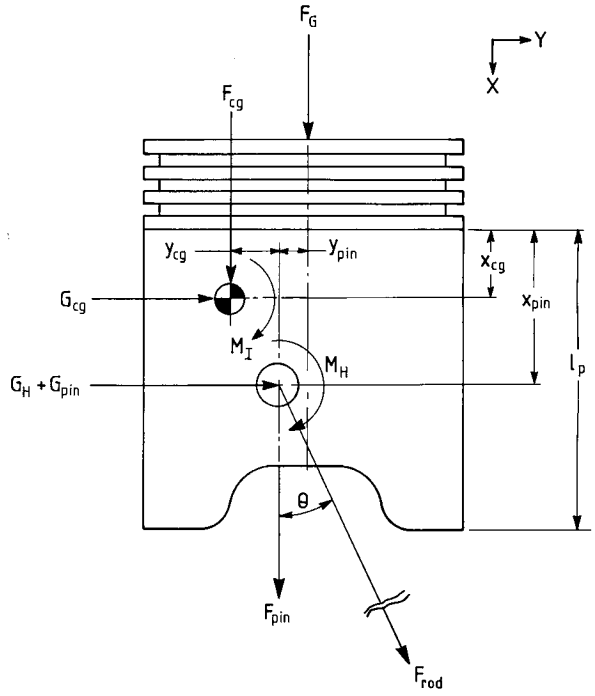

Figure 5 : Forces and Moments Considered to Act on the Piston

Unlike the piston rings analysis of the piston skirt cannot be limited to two dimensions due to the ability of oil to flow both axially and circumferentially around the piston. In addition to the assumptions of smooth surfaces and an isoviscous Newtonian fluid the influence of the ring pack upon the piston motion is regarded as negligible, and any friction due to the twisting of the piston pin is neglected as is the rotational inertia of the pin and connecting rod. For this situation the Reynolds' equation, for a fixed set of axes moving with the piston, may be written in polar coordinates as:-

$$\frac{\partial}{\partial\phi}\left(h^3\frac{\partial p}{\partial\phi}\right)+R^2\frac{\partial}{\partial X}\left(h^3\frac{\partial p}{\partial X}\right)=12\eta R^2\left[\frac{\partial h}{\partial t}-\frac{U}{2}\frac{\partial h}{\partial X}\right] \quad \ldots\ldots\ldots\ldots\ldots\ldots(29)$$

where X is in the piston axial direction, ϕ is measured around the piston circumference from the major axis, and the film thickness, h, is obtained from consideration of piston tilt and barreling present on the skirt by the approximation:-

$$h = c(X) + e_t\cos\phi + \frac{X}{l_p}(e_b - e_t)\cos\phi \qquad (30)$$

The value of c(X) represents the radial clearance along the length of the skirt when the piston is aligned in the bore, allows the variation in shape of the piston skirt to be accounted for.

To permit the inclusion of possible starvation effects it is possible to limit the area over which the Reynolds equation is solved to that in which the lubricant film is less then, or equal to, a specified value. The simultaneous solution of the resulting equations governing the dynamic and hydrodynamic action of the piston are not discussed here. However, the general method is described in Li et al [10] with details particular to these results outlined in Chittenden and Priest [7].

The results from the lubrication analysis provide knowledge of the pressures in the oil film both down the length of the skirt, in the thrust plane, and circumferentially to the boundary known as the "fluid angle". This latter limit is used to account for the regions of the skirt where the nominally cylindrical profile had been cut away. Outside this region all values are assumed to be zero. The shear stresses are readily calculated according to Newtonian theory and hence the instantaneous friction force may be found by integration.

$$f = 2R\int_0^{\ell}\int_0^{2\pi}\tau\,dX\,d\phi \qquad (31)$$

In cases where contact between the skirt and cylinder is indicated, the additional friction force is accounted for using a nominal coefficient of friction for non-hydrodynamic conditions, 0.12 for SAE 0W20 without FM, and the calculated contact force in the thrust plane.

The piston skirt model of Chittenden and Priest [7] was used to carry out the lubrication and friction loss analysis of the Ricardo Hydra piston skirt. Taking into account all the forces acting on the piston assembly, the eccentricity ratios for the top and bottom of the Ricardo Hydra piston were calculated at 2° intervals of crank angle for engine speeds of 800rpm, 1500rpm and 2000rpm. Using the piston eccentricity information, the lubricant film thickness at the top and bottom of the skirt were calculated at each crank angle, thus generating the data for the angle of piston tilt. This knowledge along with the skirt profile resulted in the film thickness variation along the skirt length. Knowing the film thickness, instantaneous piston velocity and the lubricant viscosity via local liner temperature measurement, the piston skirt frictional loss is calculated. The results of piston skirt loss predicted using both the above methods are presented in the results section.

It is recognised that there are more sophisticated numerical models for piston assembly tribology than those applied in this paper, just as there are simpler approaches. The models used here are intended for use by design analysts in OEMs, component manufacturers and lubricant companies. As such they are regarded as medium complexity numerical tools, a compromise between sophistication and usability/reliability. One major aim of this research was to judge the validity of this engineering compromise through comparison with detailed experimental data for a realistic firing engine.

5 EXPERIMENTAL MEASUREMENT OF PISTON ASSEMBLY FRICTION

Experiments were carried out on a single cylinder Ricardo Hydra gasoline engine, the design of this being based on a real engine, a GM 2.0 litre passenger car engine. The piston assembly carries two compression rings and an oil control ring. The engine specification is given in the Appendix. The piston assembly friction was measured under fired conditions using the IMEP method as it requires almost no engine modification Mufti and Priest [11].

The forces acting on the piston assembly in a real firing engine in the direction along the central axis of the cylinder liner are the gas force acting on the piston crown, piston assembly inertial force, connecting rod force, and the piston assembly friction force. Using the information from a 720 pulse per revolution encoder connected to the front end of the crankshaft and simple geometry, the direction of all the above forces can be determined. Thus if any of the three forces mentioned above are known, the fourth can be calculated. This is the basic principle of the IMEP method and was first used by Patterson [21].

Gas force is the axial force exerted by the combustion pressure on the piston assembly. It is calculated by measuring the net cylinder pressure and multiplying by the average cylinder bore area. The bore area was determined by measuring bore diameter at different locations and taking an average, 85.99 mm. The engine crankcase was open to atmospheric pressure. A Kistler 6067B water cooled piezo-electric pressure transducer having a sensitivity of 26.1 pC/bar was used to measure the gas pressure. It was flush fitted to avoid any acoustic delays and pressure drop. A separate distilled water-cooling system was developed for the pressure transducer to keep the water temperature and pressure constant and to avoid deposits in the sensor. Piezoelectric pressure transducers measure relative pressure and to relate it to an absolute value and to remove thermal drift, pressure pegging is carried out. A number of pressure referencing techniques are available and are explained by Randolph [23]. The most accurate pegging method is by using a second (absolute) pressure transducer mounted on the cylinder liner near the BDC position. Absolute cylinder pressure measurement was carried out using a Kulite XCE-152 piezo-resistive pressure transducer, figure 6. This miniature pressure transducer is 7 mm in length and 3 mm in diameter having a pressure sensing area of 1.9 mm. The miniature pressure transducer was mounted to the side of the cylinder wall such that it is not exposed to the cylinder pressure until approximately 120° after TDC position. The pressure transducer was exposed to the cylinder pressure via a 1 mm long channel having a bore of 0.5 mm, figure 7. At this point combustion is normally complete and the pressure falls to 5% to 10% of its peak value. The reading from the absolute pressure transducer was related to the cylinder pressure at 10° after BDC at the start of the compression stroke, as the pressure change in the cylinder is minimum, Brown [24].

The pressure difference is then applied to the cylinder pressure reading for the complete engine cycle.

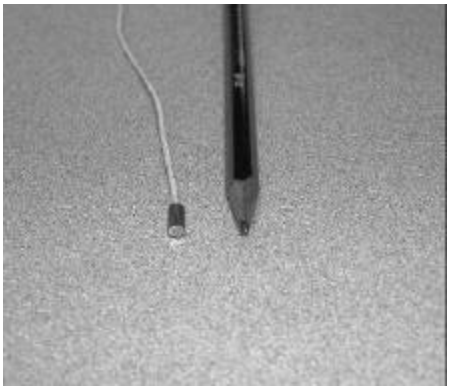

Figure 6. Piezo-resistive pressure transducer for cylinder pressure pegging

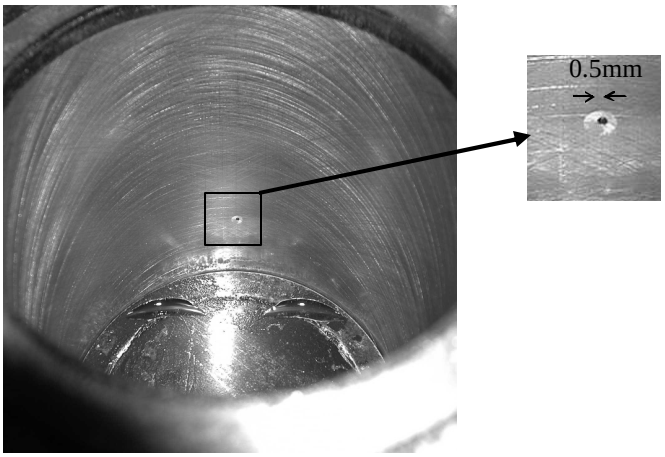

Figure 7. 1mm long and 0.5mm bore pegging channel at 120° after TDC

Instantaneous connecting rod force was measured using Micro Measurements WK-06-06TT-350 resistive type strain gauges, each having a resistance of 350Ω. The gauges were applied parallel to the neutral axis of the connecting rod stem. A full Wheatstone bridge gauge circuit was used to increase sensitivity and output voltage. The output voltage of the strain gauge circuit is directly proportional to the gauge factor, strain and excitation voltage. The orientation of the gauges in the Wheatstone bridge and on the connecting rod were such that the bridge was bending and temperature compensated. Jaguar Cars, a partner in this research, kindly carried out the finite element analysis on the connecting rod to determine the most appropriate position for installing strain gauges. A special device called a grasshopper linkage was used to lead the wires from the strain gauges on the connecting rod to the side of the crankcase figure 8.

To measure friction using the IMEP method, very accurate measurement of forces acting on the complete piston assembly is necessary including the piston assembly inertial force, As the experiments are carried out on a single cylinder 4 stroke gasoline engine, the engine speed varies throughout complete engine cycle, thus account must be given to crankshaft angular acceleration. The piston assembly axial acceleration can be calculated as,

$$\frac{d^2}{dt^2}S = -R_c \cdot \left[a \cdot \left\{ \sin(q) + \frac{l}{2} \frac{\sin(2q)}{\sqrt{1 - l^2 \cdot \sin^2(q)}} \right\} + w^2 \cdot \left\{ \cos(q) + \frac{l \cdot \cos(2q) + l^3 \sin^4(q)}{\sqrt{\left(1 - l^2 \cdot \sin^2(q)\right)^3}} \right\} \right]$$

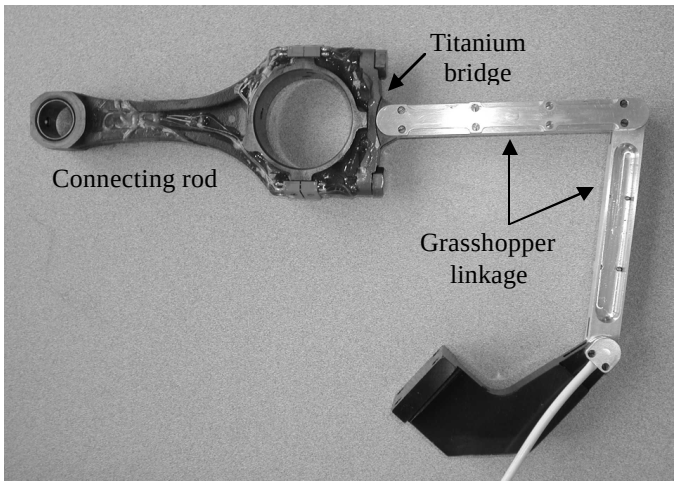

Figure 8. 24-wire grasshopper linkage.

The information from the encoder 0.5° incremental pulse and the data acquisition board timer/counter chip was used to determine crankshaft angular velocity and acceleration. An advanced data acquisition system was developed allowing the synchronized simultaneous sampling of the above data, which was vital for measuring piston assembly friction using the IMEP method.

The detail description of the IMEP method and the required instrumentation and data acquisition system can be found in Mufti and Priest [11].

Piston assembly friction measurement was carried out under fired conditions with lubricant inlet temperatures of 24°C, 40°C, 60°C and 80°C. The piston assembly friction was measured at engine speeds of 800rpm (¼ load), 1500rpm (½ load) and 2000rpm (½ load), the upper limit being defined by the capabilities of the grasshopper linkage and the vibration of the engine. For validation of the FLAME piston assembly friction model SAE 0W20 lubricant without friction modifier was used, viscosity data is given in the Appendix.

6 RESULTS

In all the graphs for instantaneous piston assembly friction presented in this paper, 0 degrees is the engine TDC fired position, start of the power stroke. A typical cyclic variation of friction force for a piston assembly at an engine speed of 800rpm is shown in figure 9. The sudden change in sign of the friction force at the end of each stroke is due to the change in direction of piston travel. Despite addressing the combustion pressure transducer drift, it was seen that at low lubricant temperature under fired conditions, the pressure transducer calibration slightly drifted at the end of the compression stroke (figure 9, between 675° and 720°), causing the friction force to

cross the zero datum line slightly. The effect was reduced considerably at higher lubricant temperatures.

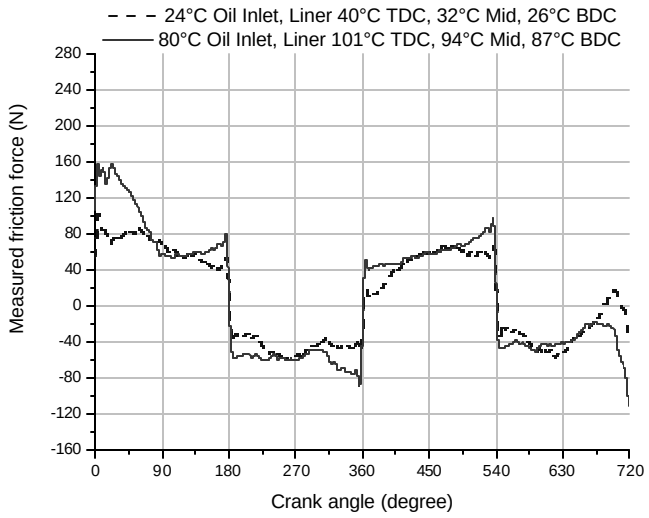

Figure 9. Measured piston assembly friction force, engine speed 800rpm, ¼ load, SAE 0W20 without FM.

At any engine operating condition, the maximum friction takes place at the start of the power stroke as the lubrication condition at this point is in the boundary regime due to the peak combustion pressure, resulting in high compression ring radial loading. At the end and start of each stroke the piston/liner friction is more towards boundary lubrication whereas at mid stroke it is generally hydrodynamic because of the relatively high entraining velocity.

While examining the friction results it is important to bear in mind that the measured piston assembly friction force is the summation of four main components: two compressions rings, an oil control ring and the piston skirt. Therefore a change in a variable may produce different and even conflicting effects for each component. For example at moderate lubricant temperatures the piston skirt operates in the hydrodynamic regime whereas the piston rings operate in the boundary to hydrodynamic lubrication regimes. Any increase in lubricant temperature would bring the piston ring lubrication conditions more towards boundary, increasing the friction loss whereas the decrease in viscosity would reduce the friction contribution from the piston skirt due to a reduction in shear loss.

Figure 9 shows the piston assembly friction at an engine speed of 800rpm for lubricant inlet temperatures of 24°C and 80°C. It can be seen that at a lubricant temperature of 24°C, at the start of the power stroke the piston assembly friction is high due to severe lubrication conditions resulting in boundary lubrication, but as the piston picks up velocity, just before and after mid stroke, the friction decreases due to a high entraining velocity dragging more lubricant into the piston/liner interface. Thus the piston/liner interface enters into the hydrodynamic lubrication regime. At mid stroke, the entraining velocity is high and under hydrodynamic lubrication conditions, this results in an increase in friction due to high shear rate (figure 9). A similar picture can be seen for other piston strokes.

At 80°C lubricant temperature, due to severe lubrication conditions, a sharp rise in friction can be seen at the start of the power stroke. Also the friction at the start and end of each stroke is high as the film thickness in this region is relatively small due to low entraining velocity and low lubricant viscosity but at mid strokes there is a slight decrease in friction. One of the main factors responsible for the difference in friction loss during upward and downward piston strokes is the flow/availability of lubricant on the liner surface, as the piston uncovers and covers the liner. The flow/availability of lubricant is also dependent on the engine speed.

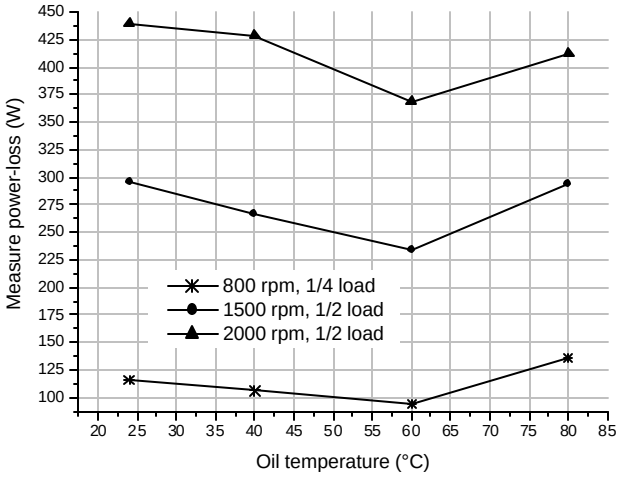

Figure 10. Measured piston assembly average power loss, SAE 0W20 without FM.

Figure 10 clearly shows the average cyclic piston assembly power loss correlating with the Stribeck curve at any engine speed.

The measured data are compared with the predicted results using the piston assembly friction model for the compression and oil control rings of Yang [8] and the model of Chittenden and Priest [7] for the piston skirt/liner interaction, described earlier. Figure 11 shows the predicted and measured instantaneous piston assembly friction at an engine speed of 800rpm and lubricant inlet temperatures of 24°C and 80°C. It is clear from these graphs that the predicted piston assembly friction results correlate very well with the measured data, especially at high lubricant temperature.

The computed friction force data for the individual components are shown in figure 12, to provide an indication of the relative importance of the friction losses associated with each element and its contribution towards total piston assembly friction. It is assumed that the oil control ring works in the boundary regime and hence the friction force is proportional to the load acting upon it. Thus the oil control ring generates more friction loss than any of the compression rings except during the start of the power stroke where the losses at the compression ring/liner interface exceed that of the oil control ring. The lubrication regime at the piston skirt and liner interface is hydrodynamic and can be seen as a nearly sinusoidal signal in figure 12.

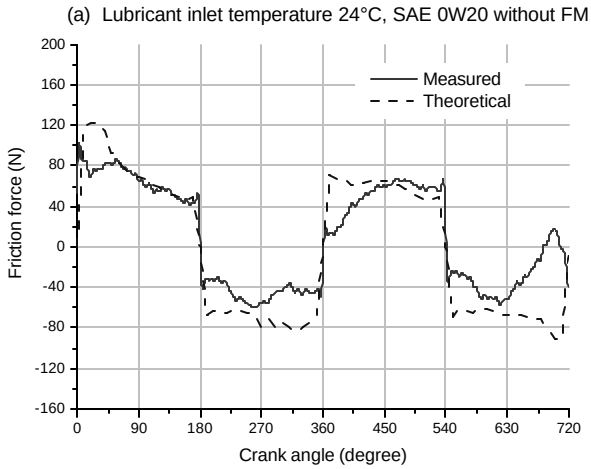

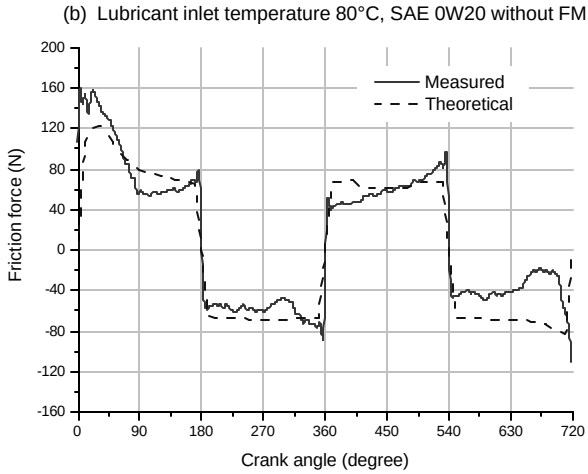

Figure 11. Predicted and experimental measurement of instantaneous piston assembly friction at engine speed 800rpm, ¼ load.

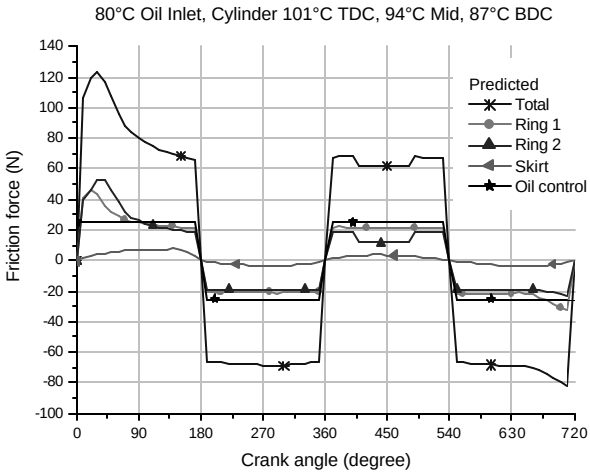

Figure 12. Predicted piston assembly component friction at engine speed 800rpm and lubricant inlet temperature of 80°C.

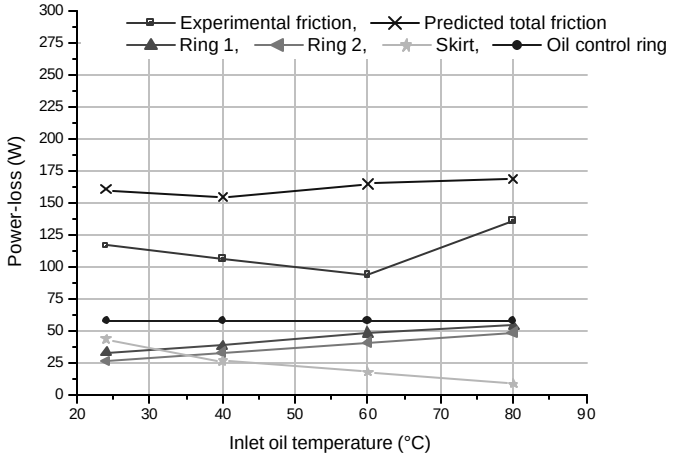

Figure 13. Predicted piston assembly component power-loss and experimental result at engine speed 800rpm, ¼ load.

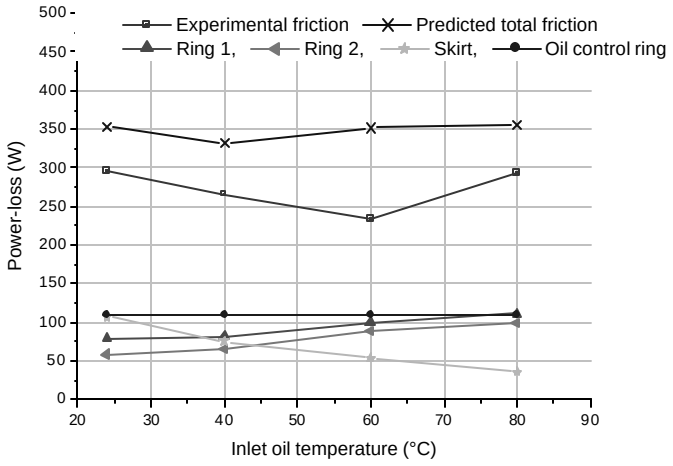

Figure 14. Predicted piston assembly component power-loss and experimental result at engine speed 1500rpm, ½ load.

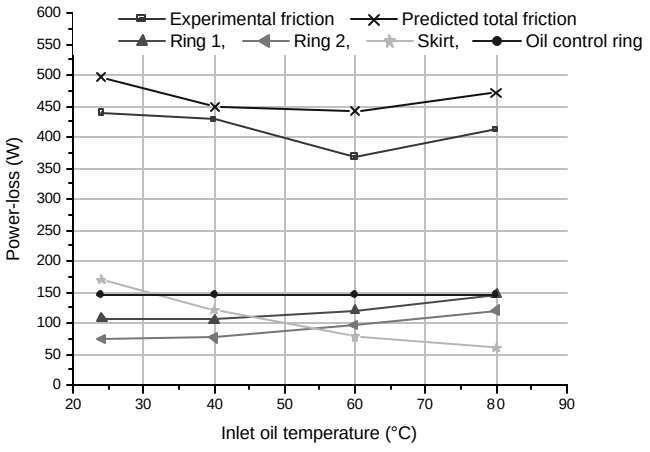

Figure 15. Predicted piston assembly component power-loss and experimental result at engine speed 2000 rpm, ½ load.

Comparing the average measured and predicted piston assembly friction power loss as shown in figures 13 to 15 it is clear that the calculated friction is qualitatively similar to the measured. The oil control ring produces the largest single contribution to the total friction loss of the piston assembly and this remains unaltered at any lubricant temperature because the assumption that boundary lubrication occurs throughout the stroke removes any lubricant viscometric influences. The role of the oil control ring is to distribute the lubricant around the circumference of the cylinder liner and to limit the lubricant flow to the compression rings. The gas pressure above and below the oil control ring is assumed to be equal to crankcase pressure and thus the only loading exerted by the control ring on the liner is due to the radial loading arising from the inherent elastic tension of the oil control ring alone. Due to the very narrow height of the oil control ring and high ring elastic tension loading, it is assumed that the asperity contact takes place and the oil control ring/liner interface operates in the boundary lubrication regime. The friction contribution from skirt/liner interaction is mainly due to shear loss, as evidenced by a continuous decrease in power-loss as lubricant temperature increases at any engine speed, figures 13 to 15. This correlates very well with the findings of Seki et al [25] who used an optical measurement technique to measure film thickness between piston and liner and found continuous oil film thickness between the skirt and the liner throughout the engine stroke.

It is clear from the above figures that the predicted compression ring friction contribution increases as lubricant temperature increases at any engine speed as the compression rings work in the boundary to hydrodynamic lubrication regimes. The lubricant supply to the compression rings plays a key role in determining the ring/liner interface lubrication condition. Oil transport is an important and complicated issue in the analysis of lubrication of ring pack and oil consumption in an engine. There are a number of factors that will affect the lubrication of the compression rings: the ring geometry; distortion of the piston and liner; the accumulation of lubricant within the ring pack; the gas flow through the pack and the dynamic behaviour of the ring, such as ring tilting. The second compression ring contributes in controlling the volume of oil available for the top ring so that sufficient oil is present to generate an adequate film to survive in extreme conditions of high gas temperature and pressure. The second ring delivers a controlled amount of lubricant to the top ring as excess lubricant will lead to high oil consumption yet too little oil will result in top ring scuffing. Thus the top ring experiences a relatively starved lubrication condition as compared to second ring.

The predicted piston assembly loss in figure 16 is calculated using two different skirt analyses, the piston/liner concentric analysis of Yang [8] and the more complex and realistic analysis that introduces piston secondary motion of Chittenden and Priest [7]. The power loss generated by the compression rings and the oil control ring is the same for both the predicted cases. The highest power loss shown in figure 16 is produced by the simple piston skirt/liner lubrication analysis assuming that the piston remains concentric with the liner throughout the engine stroke and the clearance between the piston and the liner is filled with lubricant, thus over-predicting the power loss due to high shear friction. However the result obtained by considering the secondary motion of the piston skirt correlates very well with the measured piston assembly power loss. The piston orientation at a number of crank angle positions at various engine speeds can be seen in figure 17.

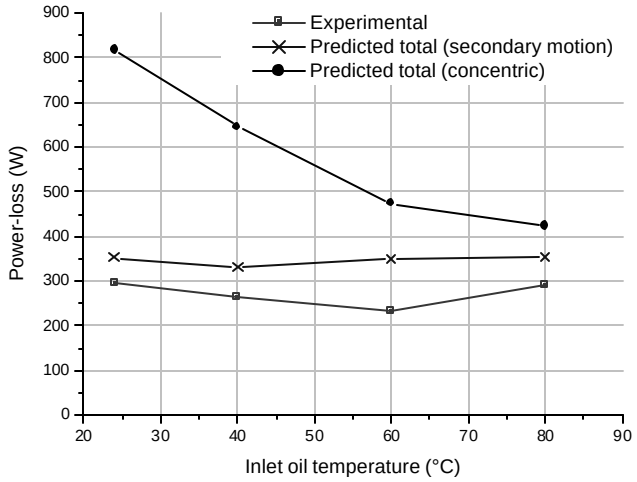

Figure 16. Comparison of the predicted piston assembly friction for two different piston skirt analysis, 1500rpm.

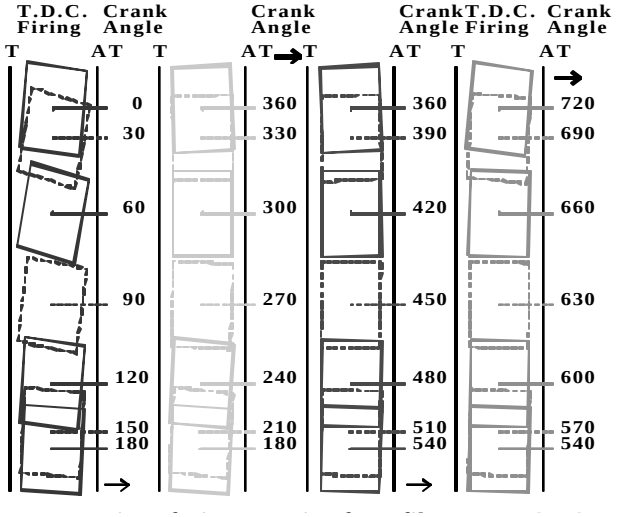

Figure 17. Piston orientation using the model of Chittenden and Priest [7], engine speed 800rpm, ½ load.

7 CONCLUSIONS

Instantaneous piston assembly friction measurement was carried out on a Ricardo Hydra single cylinder gasoline engine at different engine operating conditions using the IMEP method, which was found to be a powerful tool to monitor engine performance and lubricant evaluation. During the

experiments it was revealed the lubricant viscosity had a significant effect on the piston assembly friction.

A slight error reading for the friction was seen especially at low lubricant temperature where the piston assembly friction results showed the opposite sign at the end of the compression stroke. This is due to the drift in pressure transducer calibration, which is sensitive to environmental temperature. Using a higher resolution pressure transducer can further reduce this pressure drift. The piston assembly friction results indicate that at low lubricant inlet temperatures hydrodynamic lubrication was dominant whereas at higher inlet lubricant temperatures mixed to boundary became more influential. At any engine speed the averaged piston assembly friction data correlated very well with the Stribeck curve, a decrease and then increase in friction as lubricant temperature changed from low to higher values. During mid-stokes, the hydrodynamic lubrication contribution was higher whereas near the piston dead centres, boundary to mixed lubrication became more dominant.

Compared experimental data with predicted results, it is concluded that the predicted results correlate very well with the measured data at all engine speeds and lubricant temperatures. The piston skirt friction was predicted using both a concentric piston/liner, Yang [8] and the more realistic method of Chittenden and Priest [7], incorporating piston secondary motion. It was seen that the former over-predicted friction due to high shear loss whereas the results obtained by the latter method were better correlated to the measured results.

Overall, it was observed that the piston ring lubrication is boundary to mixed near dead centres and hydrodynamic during mid strokes whereas piston skirt friction is mostly hydrodynamic throughout the stroke.

NOMENCLATURE

A	cross section area
a_o	piston assembly acceleration
b	piston ring width
BDC	bottom dead centre
C_1-C_3	constants
c_p	specific heat at constant pressure
c_v	specific heat at constant volume
D	cylinder liner diameter
dq	crank angle increment
f	piston assembly friction
FM	friction modifier
F_{cg}	axial inertia force (N)
F_G	gas force acting on the piston crown (N)
F_{pin}	inertia force due to axial motion of piston pin (N)
F_r	viscous traction force
F_{rod}	force acting along connecting rod (N)
F_{skirt}	piston skirt power-loss
F_x	hydrodynamic pressure force in 'x' direction
F_z	hydrodynamic force
G_{cg}	transverse piston inertia force (N)
G_H	transverse hydrodynamic force (N)
G_{pin}	transverse piston pin inertia force (N)
h	height, film thickness
H_r	average friction power loss
IMEP	indicated mean effective pressure
K_c	discharge coefficient
L	connecting rod length
l_p	piston skirt length (m)
m	mass of gas
m_p	piston assembly mass
M_H	moment of hydrodynamic forces about gudgeon pin (Nm)
M_I	inertial moment about gudgeon pin (Nm)
n	refers to ring number
p	pressure
p_a	oil film pressure in inlet region of piston ring
P_{at}	atmospheric pressure
p_b	oil film pressure in outlet region of piston ring
$\overline{p_n}$	P_n / P_{at}
$(p_n)_q$	P_n at crank angle q
Q	volume flow rate per unit width
R	gas constant
R_c	crank radius
R_r	effective radius of curvature
S	piston displacement
T	temperature
T_e	piston ring elastic tension
U_r	velocity of piston ring
U_l	velocity of liner
V	volume
w_o	velocity of fluid flow entering through the bearing surface
w_h	velocity of fluid flow leaving through the bearing surface
X	normalised piston axial coordinate (=x/l_p)
x_{cg}	displacement of the piston centre of mass from the top of the skirt (m)
x_{pin}	displacement of the piston pin from the top of the skirt (m)
Y	piston radial coordinate in the thrust plane (m)
y_{cg}	displacement of the piston center line from the piston pin (m)
y_{pin}	displacement of the piston pin from the piston centre of mass (m)
a	crankshaft acceleration
r	density of gas
ϕ	piston circumferential coordinate (rads) (Note, 0° lies on the thrust plane at the major thrust side)
g	$\frac{c_p}{c_v}$
l	$\frac{R_c}{L}$
q	crank angle
h	viscosity
w	angular velocity

ACKNOWLEDGMENTS

The authors would like to thank the Engineering and Physical Sciences Research Council (UK), Federal Mogul Corporation, Ford Motor Company, Jaguar Cars Limited and Shell Global Solutions for their financial and technical support of this research. In particular, Federal Mogul Corporation for providing grasshopper linkage, Jaguar Cars Limited for carrying out finite element analysis on the connecting rod and Shell Global Solutions for the provision of the test lubricants, are gratefully acknowledged.

.

REFERENCES

[1] Dowson, D., 1993, "Piston assemblies; Background and lubrication analysis", Engine Tribology (Tribology series 26), C. M. Taylor (editor), ISBN 0444897550, pp. 213.

[2] Furuhama. S., 1959, "A dynamic theory of piston ring lubrication (1st report, calculation)", Bulletin of the J.S.M.E., Vol. 2, No 7., pp. 423-428.

[3] Lloyd, T., 1969, "The hydrodynamic lubrication of piston rings", 1969 Tribology Convention, Proc. Instn. Mech. Engrs., Vol. 183, Pt 3b, pp. 28-34.

[4] Wakuri, Y., Soejima, M., and Taniguchi, T., 1978, "On oil film behaviour of piston rings (correction of effective pressure region of oil film)", JSME Bulletin, Vol. 21, No 152, pp. 295-302.

[5] Dowson, D., Economou, P.N., Ruddy, B.L., Strachan, P.N., and Baker, A.J.S., 1979, "Piston ring lubrication – Part II, Theoretical analysis of a single ring and a complete ring pack", Energy conservation through fluid film lubrication technology: Frontiers in research and design, ed. Rohde, S.M. Wilcock, D.F. and Cheng, H.S., ASME publications, pp. 35-66.

[6] Ruddy, B.L., Dowson, D., Economou, P.N., and Baker, A.J.S., 1979, "Piston ring lubrication – Part III, The influence of ring dynamics and ring twist", Energy conservation through fluid film lubrication technology: Frontiers in research and design, ed. Rohde, S.M. Wilcock, D.F. and Cheng, H.S., ASME publications, pp. 191-215.

[7] Chittenden, R.J. and Priest, M. 1993, "Analysis of the piston assembly, bore distortion and future developments, Chapter 10, Engine Tribology, ed. Taylor C.M., Elsevier, Amsterdam.

[8] Yang, L.S., 1992, "Friction modelling for internal combustion engines", Ph.D. Thesis, Department of Mechanical Engineering, University of Leeds, UK, pgs. 230.

[9] Dickenson, A.N., 2000, "Engine Friction Modelling Considering Lubricant Tribological Characteristics", Ph.D. Thesis, School of Mechanical Engineering, University of Leeds, UK, pgs. 232.

[10] Li, D.F., Rohde, S.M., and Ezzat, H.A., 1982, "An automotive piston lubrication model",ASLE Transactions, 26(2), pp. 151-160.

[11] Mufti, R.A, and Priest, M., 2004, "Experimental evaluation of piston assembly friction under motored and fired conditions in a gasoline engine". Journal of Tribology, ASME. (submitted).

[12] Eweis, M., 1935, "Reibungs und Undichtigkeitsverluste an Kolbenringen", Forschungshefte des Vereins Deutscher Ingenieure, No. 371

[13] Ting, L.L and Mayer, J.E., 1974, "Piston ring lubrication and cylinder bore wear analysis, part I", J. Lub. Tech., Trans. ASME, Vol. 96, Ser. F, No. 3, pp. 258-266.

[14] Ruddy, B.L., Dowson, D. and Economou, P., 1981, "The prediction of gas pressure within the ring packs of large bore diesel engines", J. Mech. Eng. Sci., Vol. 23, No. 6, pp. 295-304.

[15] Kuo, T., Selinau, M., Theobald, M. and Jones, J., 1989, "Calculation of flow in the piston-cylinder-ring crevices of a homogeneous charge engine and comparison with experiment", SAE Paper 890838.

[16] Gumbel, L.K.R., 1921, "Vergleich der ergebrusse der rectinerischen behandling des lagerschmierangsproblem mit neueren versuchsergebrussen" Monatsbl. Berliner bez. Ver. Dtsch. Ing., pp. 125-128

[17] Brown, S.R. and Hamilton, G.M., 1978, "Negative pressures under a lubricated piston ring", J. Mech. Eng. Sci., Vol. 20

[18] Cameron, A., 1981, "Basic lubrication theory", 3rd edition, Ellis Horwood series in engineering science., No. 1, pp 49-57.

[19] Thring, R.H., 1989, "Piston skirt friction in internal combustion engines", Proc. Instn. Mech. Engrs., Conf. on reduction of friction and wear on combustion engines, Paper C375/002, pp 7-11.

[20] Nakayama, K., Yasutake, Y., Takiguchi, M. and Furuhama, S., 1997, "Effect of piston motion on piston skirt friction of a gasoline engine", SAE Paper 970839.

[21] Patterson, D.J., 1983, "Measurement of piston and ring assembly friction instantaneous IMEP method", SAE Paper 830416.

[22] Dursunkaya, Z., Keribar, R. and Ganapathy, V., 1994, "A model of piston secondary motion and elastohydrodynamic skirt lubrication", Jnl. Tribology. Trans. ASME., Vol. 116. pp 777-785.

[23] Randolph, A.L., 1990, "Methods of processing cylinder-pressure transducer signals to maximise data accuracy", SAE Paper 900170.

[24] Brown, W.L., 1967, "Methods for Evaluating Requirements and Errors in Cylinder Pressure Measurement", SAE Paper 670008.

[25] Seki, T., Nakayama, K., Yamada, T., Yoshida, A. and Takiguchi, M., 2000, "A study on variation in oil film thickness of a piston ring package: variation of oil film thickness in piston sliding direction", JSAE 2000, pp 315-320.

APPENDIX

RICARDO HYDRA GASOLINE ENGINE DATA

Engine Bore	85.99 mm
Engine stroke	86 mm
No. of cylinders	1
No. of valves/cylinder	2 Inlet, 2 Exhaust.
Piston rings:	2 compression rings,
1 oil control ring	
Connecting rod length	143.5mm
Crank radius	43mm
Stroke	4

Piston ring data:

	Top ring	Second ring	Oil control ring	
			First land	Second land
Ring gap (mm)	0.603	0.577	0.812	0.784
Radius of curvature (mm)	98.72	28.4	2.1	1.72
Ring height (mm)	1.496	1.493	0.521	0.521

For reference lubricant viscosities:

Parameters	SAE 0W20 without FM
Vk40 (cSt)	41.37
Vk100 (cSt)	8.07